



Water-base acrylic terpolymer as a corrosion inhibitor for SAE1018 in simulated sour petroleum solution in stagnant and hydrodynamic conditions

M. Vakili Azghandi^a, A. Davoodi^{a,*}, G.A. Farzi^a, A. Kosari^b

^a Materials and Polymers Engineering Department, Hakim Sabzevari University, Sabzevar 397, Iran

^b Materials and Metallurgical Engineering Department, Faculty of Engineering, Ferdowsi University of Mashhad, Mashhad 91775-1111, Iran

ARTICLE INFO

Article history:

Received 1 May 2012

Accepted 10 July 2012

Available online 20 July 2012

Keywords:

A. Mild steel

B. Polarisation

B. EIS

C. Acid corrosion

C. Acid inhibition

ABSTRACT

The effect of static and hydrodynamic conditions (0–2000 rpm) on corrosion inhibition of a water-base acrylic terpolymer (ATP), methyl methacrylate/butyl acrylate/acrylic acid, for SAE1018 steel in simulated sour petroleum corrosive solution (NACE 1D196) were investigated by AC/DC electrochemical tests. Increase in rotation speed accelerates the corrosion rate; however the corrosion inhibitor efficiency increases. This was attributed to the enhanced mass transport of inhibitor molecules to the metal surface. OM examinations also demonstrate that in presence of ATP, a decrease in corrosion attacks is observed. Thermodynamic calculations also showed that ATP obeys Langmuir adsorption isotherm and adsorbs chemically into the surface.

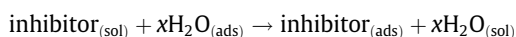
© 2012 Elsevier Ltd. All rights reserved.

1. Introduction

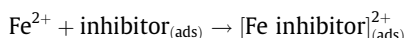
Petroleum industry is one of the most important industrial sections. Carbon steels are cheap and high strength and therefore are most applicable alloy in this industry and possibly in other industrial sections. Consequently, the study of carbon steel corrosion is important in petrochemical industries [1–4]. The oil and gas products of petrochemical industry contain some impurities such as CO₂, H₂S, O₂, H₂O, chlorides, some organic acids and bacteria. All impurities have certain influence on corrosion of carbon steels. H₂S is very soluble in water. It is 200 times more soluble than oxygen and three times more soluble than CO₂ in water at atmospheric pressure and temperature. H₂S corrodes steel, is forming various forms of iron sulfide which results in pitting corrosion. But, it was reported that the formation of iron sulphide decreases CO₂-containing petroleum solution corrosion due to formation of iron sulphides. CO₂ itself can form various structures of iron carbonate. If no liquid water is present, CO₂ is noncorrosive. Low-molecular-weight organic acids (acetic, propionic, etc.) can cause severe corrosion when exists in the petroleum at ppm levels. Chlorides produce conductive solutions on surface to form a cell for corrosive attack to occur [5–13].

The adsorption of organic molecules at the metal/solution interface is a great interest in surface science and can markedly change the corrosion resistance of the metal [14]. It is generally accepted that the first step in the adsorption of an organic inhibitor on a me-

tal surface usually involves replacement of one or more water molecules adsorbed at the metal surface [15]:



The inhibitor may then combine with freshly generated Fe²⁺ ions on steel surface, forming metal inhibitor complexes [16,17]:



Most of the well known acid inhibitors are organic compounds containing nitrogen, sulfur and/or oxygen atoms [18,19]. Recently, application of some organic polymers as corrosion inhibitor is noticeable since they have environmental friendly characteristics, are non toxic and show excellent corrosion inhibition behavior. Polymers have large chain molecules; however have less solubility and high attraction point and as a result excellent stability and corrosion inhibition [20–22]. In the present study, inhibiting performance of an environmental friendly and water-base acrylic terpolymer (ATP), methyl methacrylate, butyl acrylate, acrylic acid, was investigated. The present ATP is emulsified in aqueous solution; however use of this terpolymer as corrosion inhibitor does not need any solvent which is a great advantage as a solvent-free inhibitor. This water-base copolymer is already used in adhesive commercial resin in coating industry and so far, no study has been carried out on inhibitive performance of this compound as corrosion inhibitor in acidic media, particularly the influence of hydrodynamic conditions during rotating disc electrode (RDE) experiments. In this work, inhibition behavior of ATP on corrosion of SAE1018 steel in petroleum solution was studied by electrochemical tests

* Corresponding author. Tel.: +98 571 4003536; fax: +98 571 4003520.

E-mail addresses: davoodiali@gmail.com, adavoodi@kth.se (A. Davoodi).

such as potentiodynamic and electrochemical impedance spectroscopy and open-circuit potential. These tests were carried out in 0 (stagnant), 500, 1000, 1500 and 2000 rpm RDE speeds in absence and presence 0.1, 0.2, 0.4, 0.6 and 0.8 ppm (mmol/L) of inhibitor. Surface morphology of the polished mild steel in petroleum solution in absence and presence of inhibitor in static and hydrodynamic conditions was investigated through optical microscope (OM) imaging technique.

It should be mentioned that previous studied reported that corrosion rate in hydrodynamic conditions is different to static conditions. Very often, the increase of rotating disk electrode velocity causes an increase in corrosion rate. This was attributed to enhanced mass transport of reactant agents including aggressive ions toward metal surface. Accordingly, the corrosion inhibition behavior at hydrodynamic condition depends on adsorption of inhibitor on the surface at different rotating speed [23,24].

2. Material and experimental

2.1. Poly(methyl methacrylate/butyl acrylate/acrylic acid)

Fig. 1 represents the structure three monomers of present copolymer. The copolymer used as corrosion inhibitor in this work was a water-base acrylic terpolymer of methyl methacrylate/butyl acrylate/acrylic acid with 49:49:2 wt% ratio, respectively and containing 50 wt% water. This copolymer was produced using the free radical copolymerization mechanism and molecular weight of this terpolymer is 10^5 g/mol, the average particle size is about 160 nm and has T_g about 20 °C.

2.2. Specimen and corrosive media

The specimen (working electrode) was selected from a SAE1018 steel rod with following chemical composition (in wt%): 0.15% C, 0.6% Mn, 0.0005% B, 0.2% Cu, 0.1% Pb and Fe balance which was mounted in a polyester resin in such a way that only the end side of electrode was left uncovered, resulting in 0.785 cm² area. A home-built rotating machine was used to control the rotation speed in the range of 0 and 2000 rpm in petroleum solution in absence and presence of different inhibitor concentrations. Before each test, the specimen was ground up to 1200 grit emery paper then washed in double distilled water and dried with warm air.

The simulated petroleum corrosive solution was prepared according to NACE 1D196 standard as follows [8,25,26]:

In the first stage, the solution containing 3.5 wt% NaCl, 0.305 wt% calcium chloride and 0.186 wt% magnesium chloride hexahydrate was degassed by purging CO₂ gas with pressure of 1 atm during 1 h. After this process, the pH of solution was measured (its value was approximately 3.9). It should be noted that O₂ in a concentration more than 10 ppm reacts with H₂S, produc-

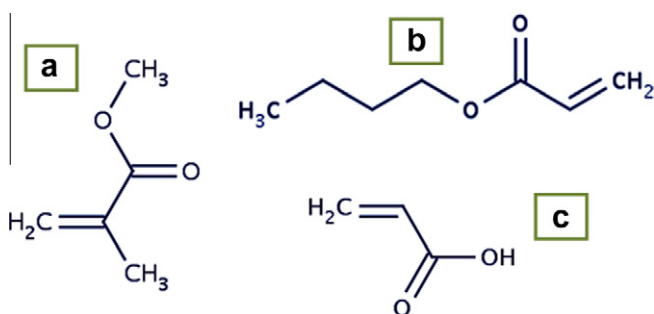


Fig. 1. Molecular structures of (a) methyl methacrylate (b) butyl acrylate (c) acrylic acid.

ing considerable H₂SO₄. Finally, CH₃COOH 1700 mmol/L and Na₂S 3530 mmol/L were added in solution in a sealed cell to generate 500 ppm H₂S and to arrive in 4.7 pH.

2.3. Electrochemical measurements

The electrochemical measurements were carried out in a conventional three-electrode cell in which the working electrode was as mentioned above and saturated calomel electrode (SCE) and a platinum wire were as reference and counter electrode, respectively. An IVIUM Potentiostat was employed to perform all electrochemical measurements. In order to reach a steady state, the working electrode was immersed in solution for 10 min. Potentiodynamic polarisation was performed with a constant sweep rate of 1 mV/s in the range of –300 to +300 mV with respect to corrosion potential. The impedance measurement was performed using AC signals with 10 mV amplitude for the frequency range from 100 kHz to 0.01 Hz at corrosion potential. EIS Analyzer software was used to fit the experimental results of EIS measurements using appropriate equivalent circuit.

2.4. Corrosion attack morphology investigation

Optical microscopy was employed to investigate the corrosion attack morphology in absence and presence of inhibitor. The specimen surface was mechanically polished down to 0.05 μm alumina slurry. Subsequently, the sample was immersed in petroleum solution in absence and presence of 0.8 ppm (mmol/L) for 15 min at room temperature in static and hydrodynamic conditions. After sample eliciting from solution, it was washed and cleaned by ethanol and immediately dried with warm air.

3. Results and discussion

3.1. Effect of concentration in static condition

3.1.1. Potentiodynamic polarisation

Anodic and cathodic polarisation curves for carbon steel, in absence and presence of various concentrations of ATP in simulated petroleum corrosive solution in static conditions, are shown in Fig. 2.

Anodic reaction is iron dissolution:

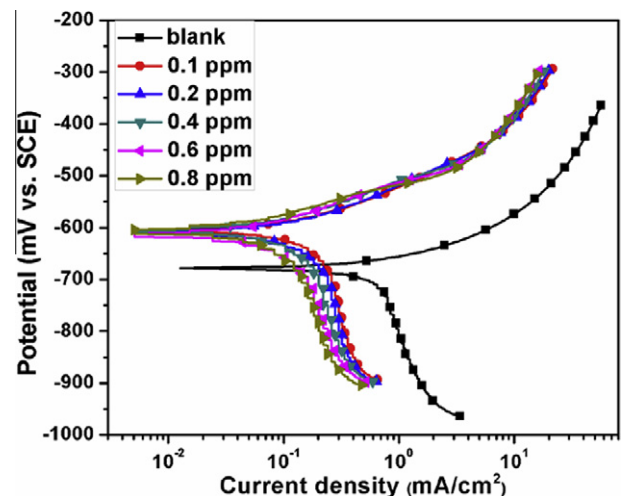


Fig. 2. Typical polarisation curves for corrosion of SAE1018 in the absence and presence of inhibitor in stagnant conditions.



It was reported that the decrease in corrosion rate of carbon steel in petroleum environment may occur due to the formation of iron sulphide (FeS) [5,9] as follows by the following reactions (in the present study, this issue has not been investigated):

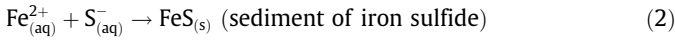
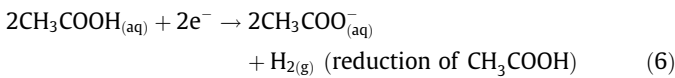
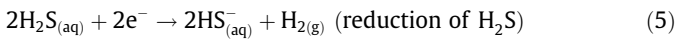
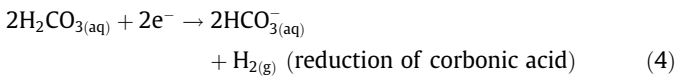
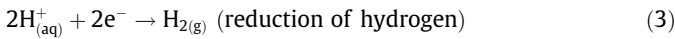


Fig. 2 shows that the current densities of anodic branches are under activation-controlled while the cathodic ones are under diffusion-controlled. As seen, the anodic current densities of inhibited solutions which are independent of inhibitor concentration are considerably lower than the uninhibited solution. In cathodic branches, the current densities decrease with increasing in inhibitor concentration. The main cathodic reactions in petroleum environment are reported as follows:



It is believed that the formation of iron sulphide on steel surface give rise to the reduction rate of mentioned species is controlled by their diffusion from bulk to the steel surface [5–7,9,10,27,28]. This topic will be deeply discussed in the EIS section.

The corrosion parameters extracted from polarisation curves containing corrosion current density (i_{corr}), corrosion potential (E_{corr}) and the anodic and cathodic Tafel slopes (β_a , β_c) have been presented in Table 1. Also, the values of surface coverage (θ) and inhibition efficiency (% η) have been calculated as a function of ATP concentration according to following equations [29,30]:

$$\theta = \frac{i_{\text{corr}}^0 - i_{\text{corr}}}{i_{\text{corr}}^0} \quad (7)$$

$$\% \eta = \theta \times 100 \quad (8)$$

Where i_{corr}^0 and i_{corr} are the corrosion current densities in absence and presence of inhibitor, respectively. It can be seen from Table 1 that the corrosion current density of carbon steel in petroleum solution considerably decreases with increasing in terpolymer concentration. This indicates that present terpolymer act as a suitable inhibitor for carbon steel corrosion. In addition, for present terpolymer the most efficient concentration found to be 0.8 ppm in which the efficiency value reaches 71%. It is believed that the decrease in corrosion rate with adding inhibitor to the petroleum solution is mainly due to the adsorption of long chains

of terpolymer onto metal surface [21,22]. Table 1 shows that the cathodic and anodic Tafel slopes remain almost constant in presence of various concentrations. This could be an indication that the addition of terpolymer does not alter the corrosion mechanism and the corrosion rate is diminished by blocking the active anodic and cathodic sites. It should be noted that the terpolymer can directly adsorb onto the surface metal. Also, it has been reported that cationic inhibitors such as present terpolymer bind to HS^- anions adsorbed on the metal surface, which act as bridges facilitating the inhibitor adsorption [21,31]. Since in presence of ATP, both anodic and cathodic current densities have been decreased, thus this compound is classified as mixed inhibitor.

3.1.2. Electrochemical impedance spectroscopy

Impedance measurements of carbon steel were performed in absence and presence of different concentrations of inhibitor in static condition at the open-circuit potentials. The influence of terpolymer concentration on impedance spectra of steel has been presented in the form of Nyquist and Bode plot in Fig. 3. The impedance spectrum for inhibited and uninhibited solutions is similar in shape and recorded values suggesting similar characteristics. The equivalent circuits proposed to fit the experimental data in static conditions have shown in Fig. 4a and b. The equivalent circuit proposed to fit the experimental data consists of solution resistance R_s in a serial connection with one time constant: $R_s(C_{dl}R_{ct}W)$ in impedance data of corrosion behavior of blank solution on static condition and two time constants: $R_s(C_{dl}R_{ct})(C_{layer}R_{layer}W)$ in presence of corrosion inhibitor. The first time constant in the high frequency region is proposed to be a result of a fast charge transfer process of steel dissolution, with R_{ct} being the charge transfer resistance. A reasonable fit of the $R_{ct}C_{dl}W$ sub-circuit is obtained when C_{dl} is replaced by a constant phase element (CPE) with the exponent, n . This impedance element is calculated by following equations [32]:

$$Z_{\text{CPE}} = [Q(j\omega)^n]^{-1} \quad (9)$$

where Q is the constant, ω is the angular frequency, and n is the CPE power.

In these electrical circuits Z_W is a finite length Warburg impedance element that represents the diffusion of reactive species. The total impedance is calculated by following equations [33,34]:

$$Z_{\text{total}} = R_s + \frac{R_{ct}}{1 + Q(j\omega)^n R_{ct}} + \frac{R_{layer}}{1 + R_{layer}j\omega C + R_{layer}O(j\omega)^{0.5} \coth[B(j\omega)^{0.5}]} \quad (10)$$

where j is the imaginary number ($j^2 = -1$), B is the diffusion factor, C is capacity and O is the finite length diffusion element. The quantitative analysis of the experimental impedance data was performed using Eq. (10) by a non-linear least squares minimization method developed by Boukamp [35]. The fit parameters obtained for various concentrations of terpolymer were extracted and analyzed. The results of this analysis were shown in Table 2. The results show that a new layer on the surface of electrode was formed by polymeric corrosion inhibitor and capacitance of layers decrease with increasing in inhibitor concentration. The significant decrease in capacitance with increasing inhibitor concentration is attributed to the formation or reinforcement of a protective film on the electrode surface, that this decrease in according to Eqs. (11), (12) was attributed to characterizations of double layers at surface [36,37].

$$C_{dl} = P^{1/n} R_{ct}^{1/n} \quad (11)$$

$$C_{dl} = \frac{\epsilon_0 \epsilon S}{d} \quad (12)$$

Table 1

Electrochemical potential dynamic polarisation parameters for SAE1018 corrosion in the absence and presence of inhibitor at stagnant conditions.

Concentration (mmol/L)	E_{corr} (mV vs. SCE)	i_{corr} (mA/cm ²)	β_a (mV/decade)	θ	$\eta\%$
Blank	-664	0.2641	97	-	-
0.1	-595	0.2077	103	0.21	21.4
0.2	-597	0.1977	96	0.25	25.2
0.4	-598	0.1409	83	0.47	46.7
0.6	-598	0.1074	76	0.59	59.4
0.8	-596	0.0985	61	0.63	62.8

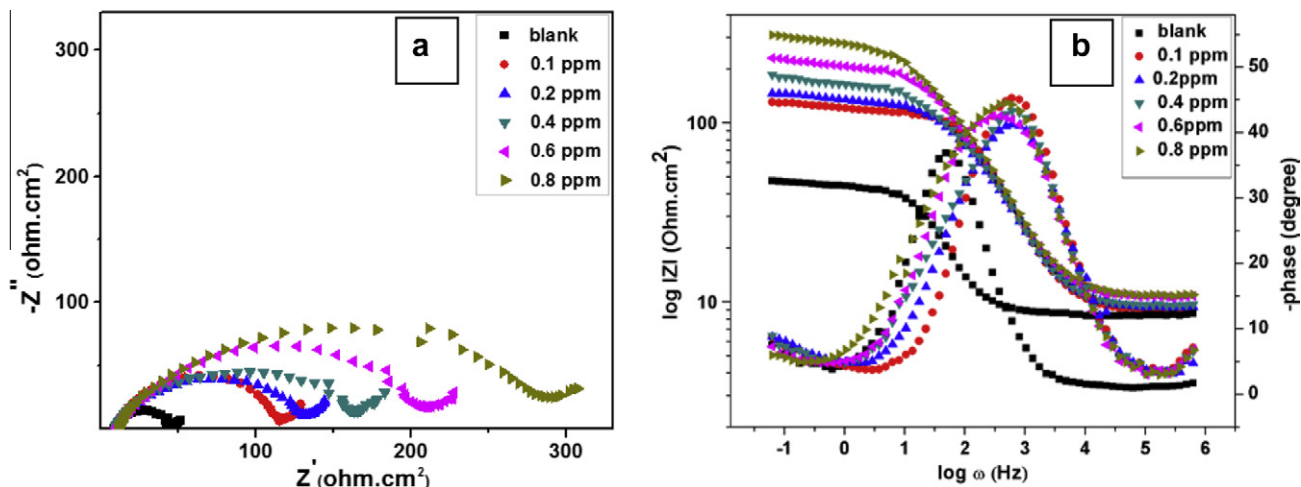


Fig. 3. Typical (a) Nyquist (b) Bode-magnitude and phase plots obtained for SAE1018 in blank and inhibited solutions at stagnant conditions.

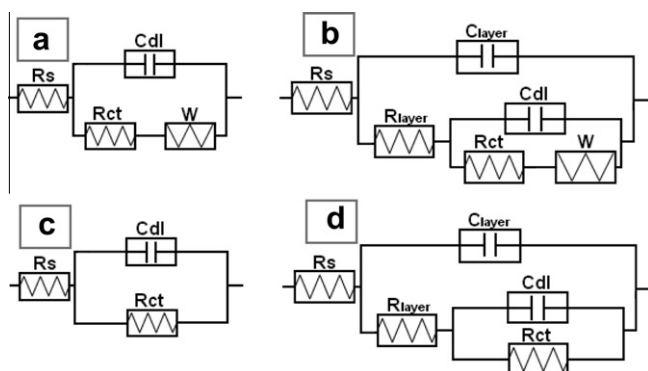


Fig. 4. The electrochemical equivalent circuits for corrosion and corrosion inhibition of SAE1018 RDE in (a) stagnant conditions in absence of inhibitor (b) stagnant conditions in presence of inhibitor (c) hydrodynamic conditions in absence of inhibitor (d) hydrodynamic conditions in presence of inhibitor.

Table 2
Electrochemical impedance spectroscopy parameters for SAE1018 corrosion in the absence and presence of inhibitor at stagnant conditions.

Concentration (mmol/l)	R_s ($\Omega \text{ cm}^2$)	R_{ct} ($\Omega \text{ cm}^2$)	R_{layer} ($\Omega \text{ cm}^2$)	θ	$\eta\%$	C_{dl} ($\mu\text{F}/\text{cm}^2$)	C_{layer} ($\mu\text{F}/\text{cm}^2$)
Blank	9.0	33.0	–	–	–	320	–
0.1	9.0	81.6	21.4	0.69	68.6	88	724
0.2	9.3	98.4	22.4	0.73	73.2	79	417
0.4	9.4	103.3	46.2	0.78	77.9	73	285
0.6	10.6	110.1	79.3	0.83	82.9	63	145
0.8	10.4	110.5	163.6	0.88	87.9	58	143

where P , n and R_{ct} are the magnitude of the constant phase element (CPE), deviation parameter and charge transfer resistance of mild steel respectively and d is the thickness of the film, S is the surface of the electrode, ϵ_0 is the permittivity of the air and ϵ is the local dielectric constant. The decrease in C_{dl} is probably due to a decrease in local dielectric constant and/or an increase in the thickness of a protective layer at electrode surface in presence of inhibitor [38]. Although by increasing in inhibitor concentration, a decrease of the surface area acting as a place for charging may also be as other reason for C_{dl} decreasing [39].

The results of impedance measurement show that the total resistance of the system (R), i.e. the sum of R_{ct} and R_{layer} values in-

creases with increasing in inhibitor concentrations. The change in total shape of impedance diagrams in absence and presence of inhibitor can be related to the change in the protective layers containing the polymeric layer and the charge transfer surface layer which have been reinforced in presence of acrylic terpolymer. The total resistance of the system was used to calculate the inhibitor efficiency for inhibitor [40]:

$$\% \eta = \frac{R - R^0}{R} \times 100 \quad (13)$$

where R and R^0 represent the total resistance with and without the inhibitor, respectively. The inhibitor efficiency of terpolymer as a function of the inhibitor concentration is presented in Table 2.

3.2. Effect of hydrodynamic condition

3.2.1. Potentiodynamic polarisation

Fig. 5 shows typical potentiodynamic polarisation curves of SAE 1018 samples in uninhibited and inhibited solutions at different hydrodynamic conditions. The electrochemical parameters including corrosion current density (i_{corr}), corrosion potential (E_{corr}) extracted from the polarisation curves and also the inhibition efficiency calculated by Eq. (8) have been presented in Table 3.

In hydrodynamic condition, the anodic sub-process, dissolution of iron, is considered as an activation-controlled reaction, while the cathodic ones are considered to be under diffusion-controlled. This is pronounced when the limiting current density (i_L) is plotted as a function of $\omega^{0.5}$ (ω is the angular frequency of rotation of the disc) according to Levich equation as follows [41]:

$$i_L = 0.62nFD^{2/3}\omega^{1/2}\nu^{-1/6}C^0 \quad (14)$$

where n is the number of electrons transferred, ν is the kinematic viscosity of the electrolyte and D is the diffusion coefficient of the reacting species of bulk concentration (C^0). Almost, linear relationships could be observed in all uninhibited and inhibited solutions in Fig. 6, this can be an indication of diffusion-controlled process. It should be noted that some features of mixed-controlled is observed in cathodic branches of high rotation speeds (i.e. 1500 and 2000 rpm), but they are also considered to be under diffusion-controlled because mixed-controlled is established in a small part of these cathodic curves and it has a minor effect on measuring corrosion rate. As observed in Fig. 5, the current density of cathodic branches in inhibited and uninhibited solutions increase with increasing in rotation speed so that the current density of cathodic

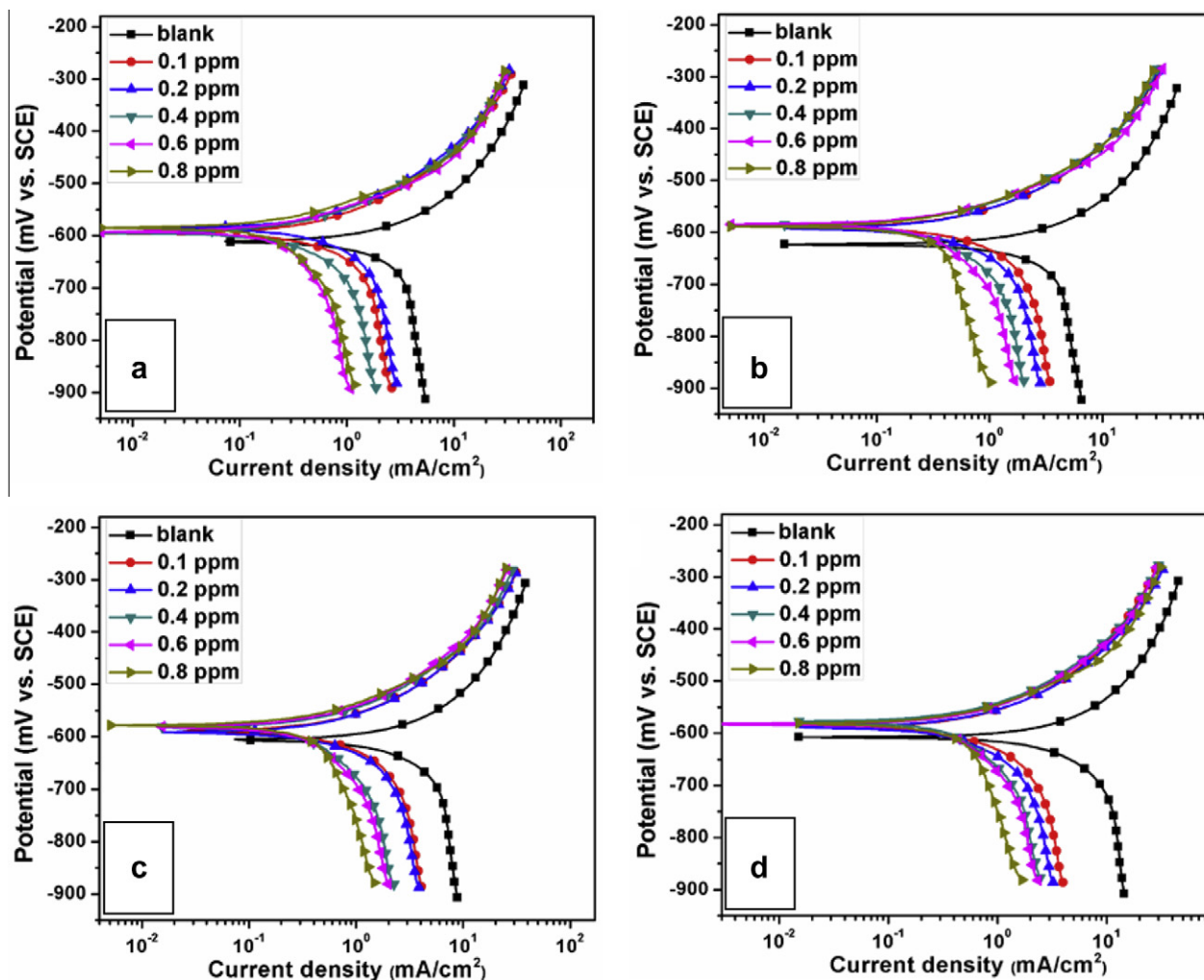


Fig. 5. Typical polarisation curves for corrosion of SAE1018 in the absence and presence of inhibitor in hydrodynamic conditions. (a) 500 rpm, (b) 1000 rpm, (c) 1500 rpm and (d) 2000 rpm.

Table 3

Electrochemical potential dynamic polarisation parameters for SAE1018 corrosion in the absence and presence of inhibitor at different rotation speeds.

Rotation speed (rpm)	Reynolds numbers	Concentration (mmol/l)	E_{corr} (mV vs. SCE)	i_{corr} (mA/cm ²)	β_a (mV/decade)	θ	$\eta\%$
500	1433	Blank	-612	3.17	162	-	-
		0.1	-591	1.46	204	0.54	53.9
		0.2	-583	1.44	156	0.54	54.5
		0.4	-591	0.94	140	0.70	70.4
		0.6	-593	0.50	100	0.84	84.3
		0.8	-585	0.49	91	0.83	85.1
1000	2865	Blank	-623	3.71	191	-	-
		0.1	-587	1.81	187	0.51	51.0
		0.2	-590	1.48	183	0.60	60.2
		0.4	-586	1.10	171	0.70	70.4
		0.6	-585	0.78	105	0.79	79.0
		0.8	-589	0.54	109	0.85	85.3
1500	4298	Blank	-607	5.49	270	-	-
		0.1	-585	2.21	208	0.60	59.6
		0.2	-587	1.61	202	0.64	64.2
		0.4	-582	1.13	182	0.79	79.4
		0.6	-581	0.95	166	0.83	82.6
		0.8	-578	0.62	142	0.89	88.7
2000	5731	Blank	-608	9.27	356	-	-
		0.1	-586	2.31	219	0.78	78.2
		0.2	-586	1.97	204	0.83	82.6
		0.4	-577	1.23	201	0.87	86.7
		0.6	-582	1.20	205	0.88	87.8
		0.8	-581	0.61	110	0.93	93.3

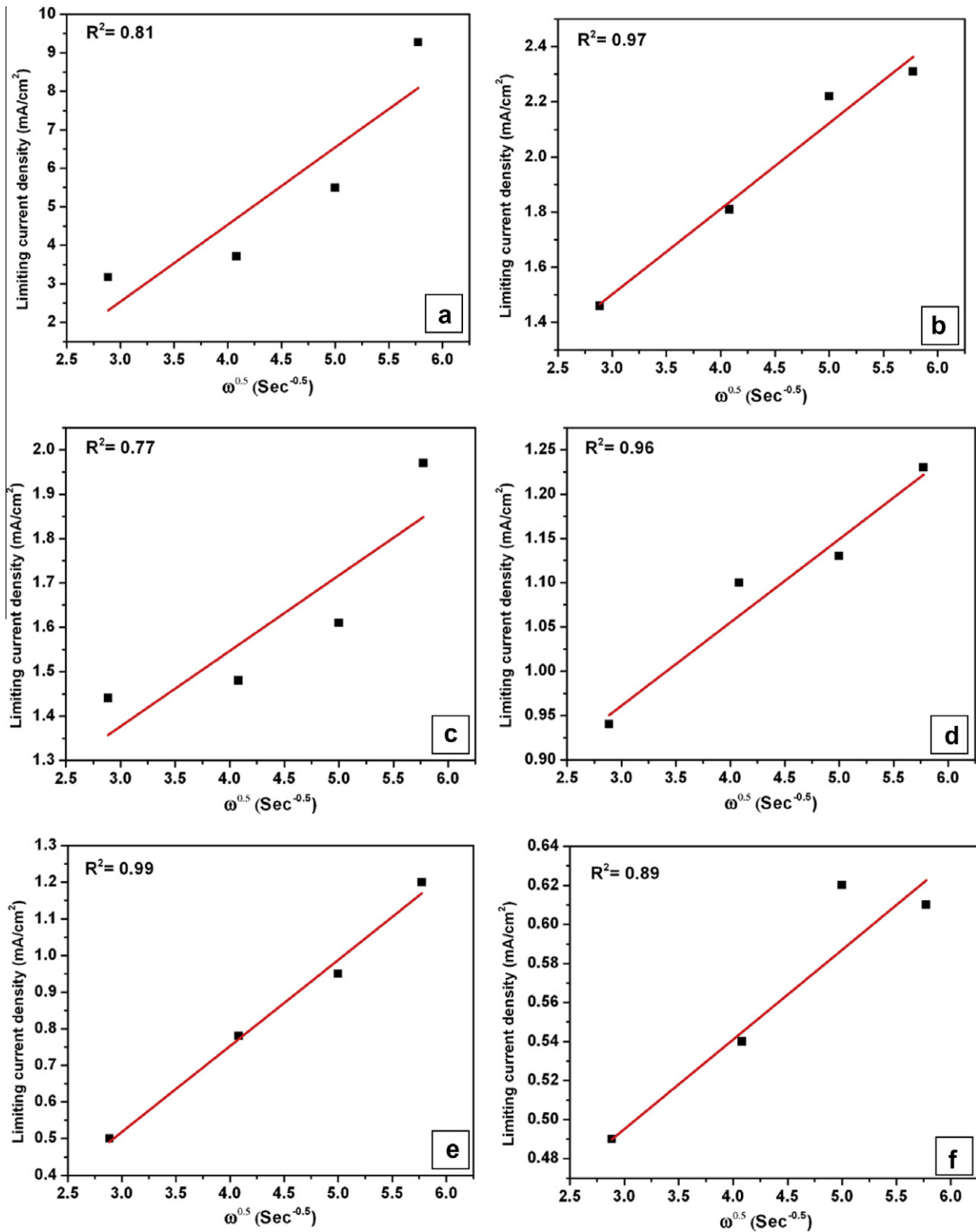


Fig. 6. LeVich plot (i_L vs. $\omega^{0.5}$) for SAE 1018 mild steel at (a) blank solution (b) 0.1 ppm (c) 0.2 ppm (d) 0.4 ppm (e) 0.6 ppm and (f) 0.8 ppm inhibitor concentration.

branches in uninhibited solution is always higher than inhibited ones in various hydrodynamic conditions. The increase in cathodic limiting current densities of uninhibited and inhibited solutions with rising in rotation speed is because of increasing in mass transfer of species which participate in cathodic reactions from bulk to surface [42]. From Table 3, it is clear that the corrosion current density of SAE 1018 in petroleum solution increases under hydrodynamic

conditions in comparison with stagnant solution. It can be also seen from Tables 1 and 3 that the presence of terpolymer in stagnant solution (0 rpm) and hydrodynamic solutions decreases corrosion current densities (i_{corr}) and shifts the E_{corr} toward more positive potentials. This terpolymer is known as mixed anodic and cathodic inhibitor in stagnant and hydrodynamic conditions, which acts through prevention of anodic dissolution of metal and cathodic reac-

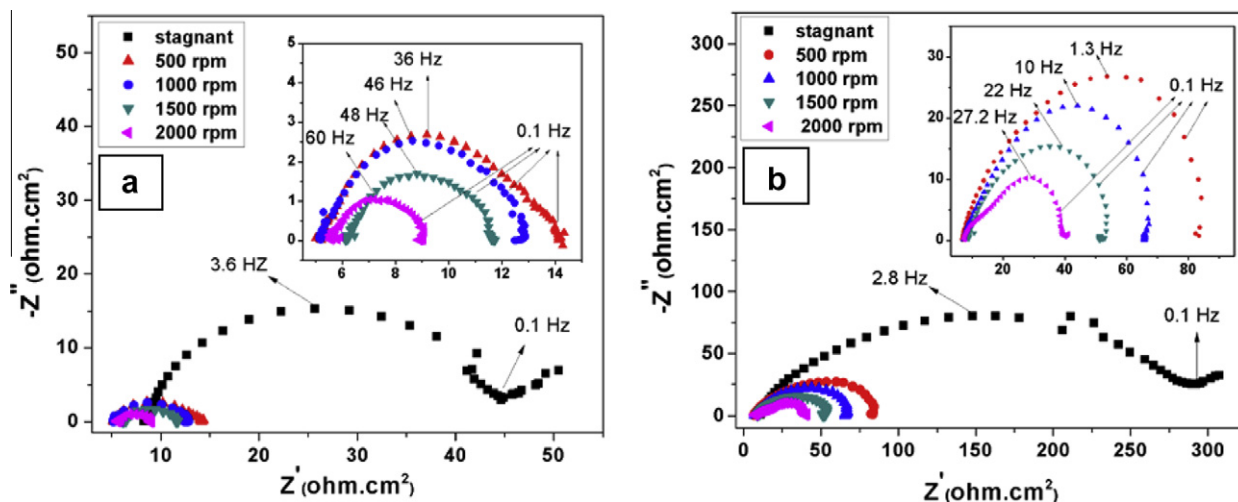


Fig. 7. Typical Nyquist plots obtained for SAE1018 RDE in stagnant and hydrodynamic conditions in (a) blank and (b) inhibited solutions in optimum concentration.

Table 4

Electrochemical impedance spectroscopy parameters for SAE1018 corrosion in the absence and presence of inhibitor at different rotation speeds.

Rotation speed (rpm)	Concentration (mmol/l)	R_s (Ω cm 2)	R_{ct} (Ω cm 2)	R_{layer} (Ω cm 2)	θ	$\eta\%$	C_{dl} (μ F/cm 2)	C_{layer} (μ F/cm 2)
500	Blank	5.1	8.7	–	–	–	553	–
	0.1	6.1	14.8	30.2	0.81	80.6	115	366.9
	0.2	5.8	15.4	34.0	0.82	82.4	87	246.3
	0.4	5.8	15.4	35.2	0.83	82.8	87	249.9
	0.6	6.2	40.0	19.0	0.85	85.2	60	300.4
	0.8	6.8	30.3	34.7	0.87	86.6	99	176.6
1000	Blank	5.1	7.9	–	–	–	645	–
	0.1	6.8	8.6	30.0	0.80	79.5	39	345.3
	0.2	6.8	10.0	29.0	0.80	79.7	46	247.3
	0.4	6.6	24.9	29.7	0.85	85.5	52	234.3
	0.6	5.8	24.1	34.3	0.86	86.4	37	169.5
	0.8	6.8	30.3	34.8	0.88	87.8	99	167.4
1500	Blank	6.1	5.6	–	–	–	944	–
	0.1	6.9	10.9	21.8	0.83	82.8	49	485.2
	0.2	7.4	9.9	22.7	0.83	82.8	61	411.2
	0.4	7.0	14.7	23.2	0.85	85.2	73	324.0
	0.6	8.0	18.0	24.0	0.87	86.6	83	365.9
	0.8	8.3	28.4	19.3	0.88	88.2	89	156.7
2000	Blank	5.5	3.6	–	–	–	924	–
	0.1	7.7	13.0	17.0	0.88	87.9	62	546.8
	0.2	6.0	10.9	19.8	0.88	88.2	77	485.8
	0.4	5.9	13.2	19.9	0.89	89.0	81	342.6
	0.6	7.4	12.8	19.6	0.89	88.8	90	252.5
	0.8	6.8	15.4	23.9	0.91	90.8	95	288.7

tions due to blocking of active surface and decrease in reaction agents in solution [43]. However, hydrodynamic conditions may also affect the inhibition of metal corrosion. It is clear from data presented in Table 3 that current density has been increased in blank and inhibited solutions with increasing rotation speed, which can be attributed to enhance in mass transport of reduction agents rather than anodic dissolution species (cations). This can be verified by the fact that the current densities of anodic branches show little increase with increasing rotation speed. But an increase in efficiency at hydrodynamic conditions can be attributed to the enhanced mass transport of inhibitor molecules to the metal surface with increase in speed and can be attributed to improving in cooperative action of adsorption of inhibitor and anion species in high rotation speed. It was reported that anions such as Cl^- can operate as bridge between inhibitor chain and metal surface. This effect can be seen in polarisation curves in which in the presence of inhibitor, anodic current density and especially cathodic current density have decreased the total current density in hydrodynamic condition more than stagnant con-

ditions. Also, the current density at hydrodynamic conditions is dependent to inhibitor concentration and it decreases with increasing in inhibitor concentration. In fact, hydrodynamic conditions may have two effects on inhibition performance [23,24,44]: (i) Flow can increase mass transport of inhibitor molecules toward metal surface, which causes the formation of more protective layers (FeS and inhibitor layer) on metal surface. This effect can improve the inhibitor performance. (ii) The high shear stress resulted from high velocity can also separate the protective films from metal surface, as a results the inhibition efficiency decrease. The balance of above mentioned effects lead to the changes of inhibition efficiency with electrode rotation rate. The reason of little change of efficiency in high rotation speed is attributed to the negative effect of the high shear stress resulted from high velocity.

3.2.2. Electrochemical impedance spectroscopy

The EIS results of inhibited and uninhibited solutions at various hydrodynamic conditions have been presented in Fig. 7, the inhib-

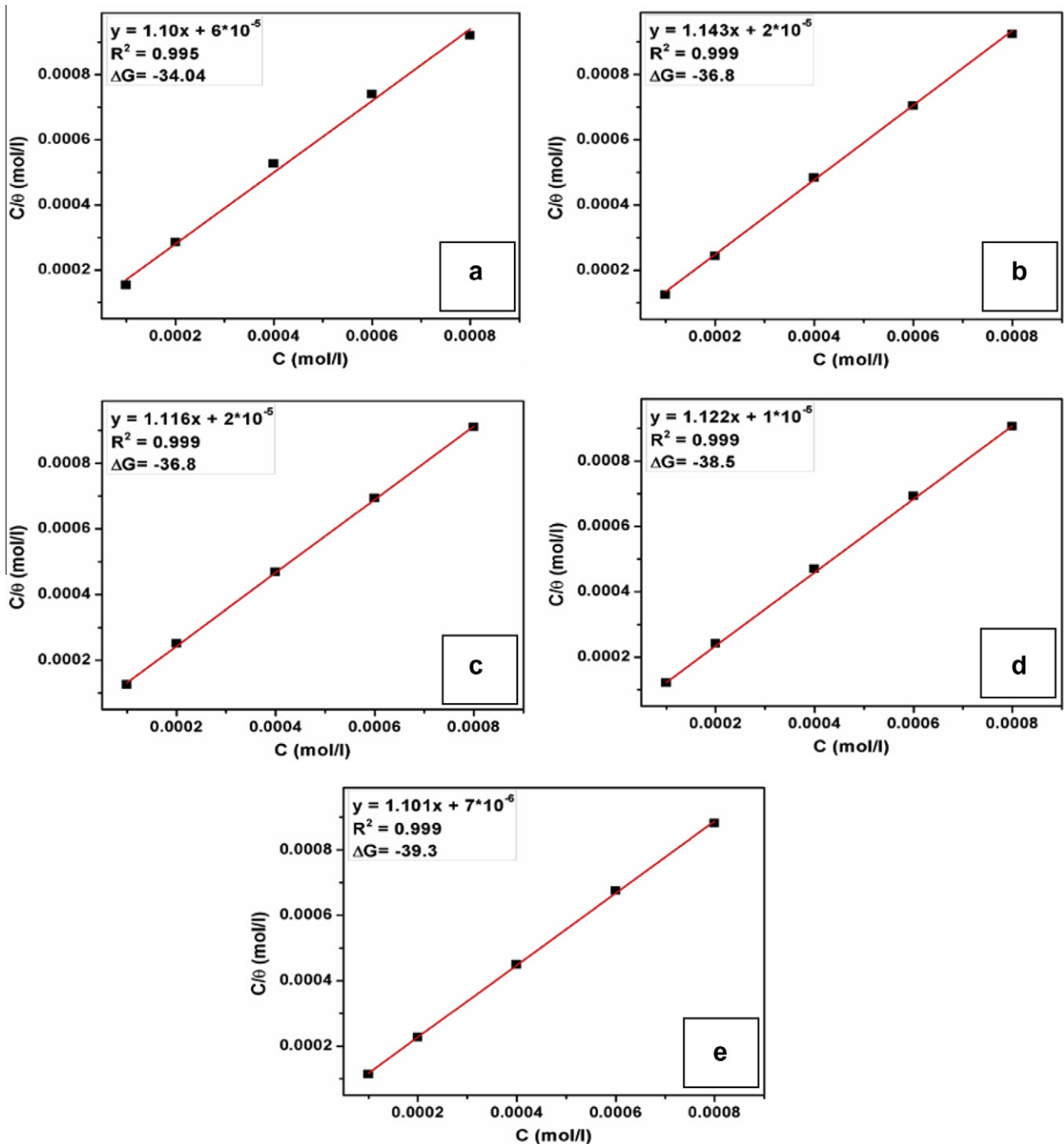


Fig. 8. Langmuir adsorption isotherm of inhibitor in petroleum solution at (a) stagnant (b) 500, (c) 1000, (d) 1500 and (e) 2000 rpm.

ited solution was prepared by 0.8 ppm concentration of ATP. Evaluation of physical parameters concerning corrosion process is discussed using an electric equivalent circuit model for the metal-solution interface. When the steel electrode is immersed in the petroleum solution in various rotation speeds, the Nyquist plots show a depressed capacitive loop, which have an asymmetrical form like stagnant condition but does not have Warburg tail. The reasons of this phenomenon can be attributed to diminishing the thickness of diffusion layer and enhancing in mass transfer of reduction agents under hydrodynamic conditions [45]. An appropriate equivalent circuit for blank solution in hydrodynamic conditions is shown in Fig. 4c in which R_s is solution resistance, R_{ct} is

charge transfer resistance and CPE_{dl} is constant phase element related to the double layer capacitance. The values of double layer capacitance have been calculated by Eq. (11).

Similar to the blank solution in presence of inhibitor in different rotation speeds, the Nyquist plot shows a depressed asymmetrical capacitive loop. Thus, the equivalent circuit shown in Fig. 4d was used to fit these spectra in which R_s is solution resistance, R_{ct} and R_{layer} are charge transfer and polymeric layer resistances, respectively. In addition, CPE_{dl} and CPE_{layer} are constant phase element related to the double layer and polymeric layer capacitance. By fitting the experimental data at all rotation rates, impedance parameters have been obtained and listed in Table 4. It can be seen from

EIS results that in blank solution the R_{ct} values are decreased as the electrode rotation rate increases which is in agreement with the polarisation results. A similar trend is observed in presence of inhibitor that can be attributed to enhance in mass transfer of cathodic agent from solution toward surface [42]. The inhibition efficiencies can also be calculated from R values using the Eq. (13). It is clear from data presented in Table 4 that addition of inhibitor has formed a new resistance layer on the surface by terpolymer and has increased charge transfer resistance of surface double layer. An increase in inhibitor concentration has increased resistances and has decreased capacities of surface layer. As described in previous section, fluid flow has several effects on the behavior of inhibitor. It can improve the performance of inhibitor through increasing the mass transport, and worsen the inhibition action by separation of protective films. The balance of these opposite effects leads to the overall changes of inhibition efficiency with rotation rate. Therefore, as the electrode rotates, the increase of inhibitor supply on metal surface cause an increase in inhibition efficiency. Under these circumstances, the beneficial effects of flow are dominant and an increase in $n\%$ is observed. But at higher speeds the interference of high shear stresses causes a little increase in inhibition efficiencies [23,24,44,46,47].

3.3. Adsorption isotherm

Adsorption isotherms provide information about the interaction among the adsorbed molecules themselves and also their interactions with the electrode surface. The adsorption free energy ($-\Delta G_{ads}$) reflects a spontaneous capacity of inhibitor molecule adsorbed on the surface of the metal, which is less than 20 kJ mol^{-1} for spontaneous physical adsorption, and is more than 40 kJ mol^{-1} for the chemical adsorption and between these is composited of chemical and physical adsorption [48], linear relation of C and C/θ in Fig. 8 in stagnant and various speeds of rotating disk electrode show that present acrylic terpolymer obeys Langmuir isotherm in

static and hydrodynamic conditions and free energy calculated from the following equations [49]:

$$\frac{C}{\theta} = \frac{1}{K_{ads}} + C \quad (15)$$

$$\Delta G_{ads}^{\circ} = -RT \ln(55.5K_{ads}) \quad (16)$$

where θ is the degree of coverage on the metal surface, C is the inhibitor concentration (mol/L), and K is the equilibrium constant. Since the experimental concentration unit is mmol/L, Eq. (15) would be transferred to correspond with them. $-\Delta G_{ads}$ is calculated. The calculated $-\Delta G_{ads}$ values at different rotation speed was $35\text{--}40 \text{ kJ mol}^{-1}$ that was greater than 20 kJ mol^{-1} and near to 40 kJ mol^{-1} . This shows that the terpolymer adsorbed on the surface of mild carbon steel in petroleum medium is composited of chemical and physical adsorption at $25 \text{ }^{\circ}\text{C}$ in static and hydrodynamic conditions.

3.4. Corrosion attack morphology

The surface morphology of the SAE 1018 sample immersed in inhibited and uninhibited (blank) solutions for 15 min, was studied by optical microscopy and the metallographic result were presented in Fig. 8. The polished surface of mild steel immersed in blank solution was rough and severely corroded in static and hydrodynamic conditions and several pits are dispersedly observed at the surface in hydrodynamic conditions (Fig. 9(a and b)). While in the case of inhibited solution (Fig. 9(c and d)), a less corrosion attack is observed and specimen surface is nearly unchanged. In micrograph of inhibited solution in hydrodynamic solution, pearlite phase has been partially etched and the grain boundary of ferrite phase is not observed. While in the case of inhibited solution in static condition is quite unchanged. These micrographs confirm result of electrochemical test in different conditions [50].

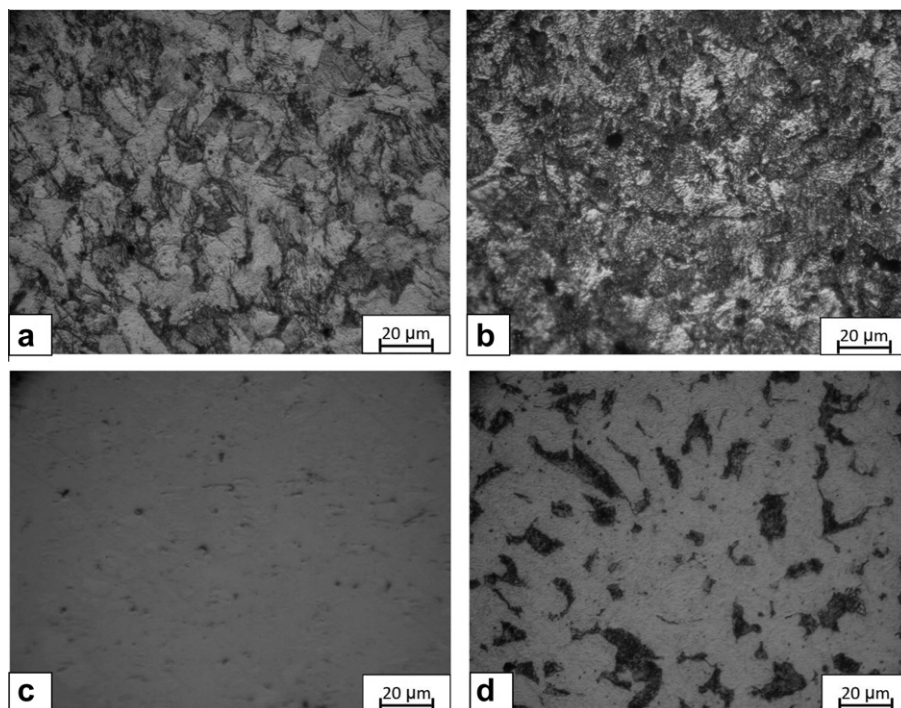


Fig. 9. Optical microscopy images in presence of (a) blank solution in stagnant conditions, (b) blank solution in hydrodynamic conditions (c) inhibited solution in stagnant conditions (d) inhibited solution in hydrodynamic conditions.

4. Conclusion

1. Addition of the acrylic terpolymer methyl methacrylate/butyl acrylate/acrylic acid (ATP) to the petroleum solution inhibited the corrosion of SAE 1018. The inhibition is due to the adsorption of this compound on the surface of mild steel.
2. Polarisation measurements showed that the ATP functions as mixed type inhibitor.
3. The inhibition efficiencies of ATP increased with increasing velocity of work electrode, which could be attributed to increasing in mass transport of terpolymer.
4. EIS measurements recorded for SAE 1018 in the petroleum solution in the absence and presence of the ATP inhibitors in static conditions showed that the Nyquist diagrams consist of a large capacitive loop in blank and two capacitive loops in inhibited solutions. It determines that ATP despite increases charge transfer resistance of double layer on the surface, form a polymeric layer on the surface electrode.
5. Adsorption on present inhibitor obeys Langmuir isotherm and thermodynamic data extracted by this rule is showing most likely chemically adsorption process in static and hydrodynamic conditions.
6. Optical microscopy obviously shows that SAE 1018 surface severely corrode in the hydrodynamic conditions into static conditions in absence and presence of ATP. And it depicts that the corrosion attack decreases in presence of inhibitors in petroleum solution in static and hydrodynamic conditions.

Acknowledgments

The authors would like to acknowledge Hakim Sabzevari University for financial support and providing experimental facilities to perform the experiments.

References

- [1] P. Altoé, G. Pimenta, C.F. Moulin, S.L. Díaz, O.R. Mattos, Evaluation of oilfield corrosion inhibitors in CO₂ containing media: a kinetic study, *Electrochim. Acta* 41 (1996) 1165–1172.
- [2] R. Cabrera-Sierra, I. García, E. Sosa, T. Oropeza, I. González, Electrochemical behavior of carbon steel in alkaline sour environments measured by electrochemical impedance spectroscopy, *Electrochim. Acta* 46 (2000) 487–497.
- [3] L. Garveric, Corrosion in the Petrochemical Industry, ASM International, USA, 1994.
- [4] P.R. Roberge, V.S. Sastri, Laboratory and field evaluation of organic corrosion inhibitors in sour media, *Corros. Sci.* 35 (1993) 1503–1513.
- [5] B. Brown, K.L. Lee, S. Nescic, Corrosion in multiphase flow containing small amounts of H₂S, in: NACE international, Biloxi, 2003.
- [6] B. Brown, S. Reddy Parakala, S. Nescic, CO₂ corrosion in presence of trace amounts of H₂S, in: NACE international, Orlando, 2004.
- [7] J. Kvarekval, The influence of small amounts of H₂S on CO₂ corrosion of iron and carbon steel, in: Eurocorr97, Trondheim, Norway, 1997.
- [8] N. International, Control of Internal Corrosion in Steel Pipelines and Piping Systems, in: Standard Practice, NACE international, Houston, 2006.
- [9] M. Singer, B. Brown, A. Camacho, S. Nescic, Combined effect of CO₂, H₂S and acetic acid on bottom of the line corrosion, in: NACE International, Milwaukee, 2007.
- [10] A. Valdes, R. Case, M. Ramirez, A. Ruiz, The effect of small amounts of H₂S on CO₂ corrosion of a carbon steel, in: NACE International, Rapid City, 1998.
- [11] H. Byars, Corrosion control in petroleum production, NACE International Niagara Falls, 1999.
- [12] J. Crolet, N. Thevenot, A. Dugstad, Role of free acetic acid on the CO₂ corrosion of steels, *Corros. J.* 99 (1999) 21–25.
- [13] R.A. Pisigan, J.E. Singley, Evaluation of water corrosivity using the Langelier index and relative corrosion rate models, *Mater. Performance* 24 (1985) 26–34.
- [14] R. Solmaz, G. Kardaş, M. Çulha, B. Yazıcı, M. Erbil, Investigation of adsorption and inhibitive effect of 2-mercaptothiazoline on corrosion of mild steel in hydrochloric acid media, *Electrochim. Acta* 53 (2008) 5941–5952.
- [15] J.O. Bockris, D.A.J. Swinkels, Adsorption of naphthalene on solid metal electrodes, *J. Electrochem. Soc.* 111 (1964) 743–748.
- [16] V. Branzoi, F. Branzoi, M. Baibarac, The inhibition of the corrosion of Armcro iron in HCl solutions in the presence of surfactants of the type of *N*-alkyl quaternary ammonium salts, *Mater. Chem. Phys.* 65 (2000) 288–297.
- [17] E.E. Oguzie, Y. Li, F.H. Wang, Corrosion inhibition and adsorption behavior of methionine on mild steel in sulfuric acid and synergistic effect of iodide ion, *J. Colloid Interface Sci.* 310 (2007) 90–98.
- [18] F. Bentiss, M. Lebrini, M. Lagrenée, M. Traisnel, A. Elfarouk, H. Vezin, The influence of some new 2,5-disubstituted 1,3,4-thiadiazoles on the corrosion behaviour of mild steel in 1 M HCl solution: AC impedance study and theoretical approach, *Electrochim. Acta* 52 (2007) 6865–6872.
- [19] M.A. Migahed, A.M. Abdul-Raheim, A.M. Atta, W. Brostow, Synthesis and evaluation of a new water soluble corrosion inhibitor from recycled poly(ethylene terephthalate), *Mater. Chem. Phys.* 121 (2010) 208–214.
- [20] S.A. Ali, M.T. Saeed, Synthesis and corrosion inhibition study of some 1,6-hexanediamine-based *N,N*-diallyl quaternary ammonium salts and their polymers, *Polymer* 42 (2001) 2785–2794.
- [21] R.R. Annand, R.M. Hurd, Adsorption of monomeric and polymeric amino corrosion inhibitors on steel, *J. Electrochem. Soc.* 112 (1965) 138–144.
- [22] S.A. Umoren, Polymers as corrosion inhibitors for metals in different media, *J. Open Corros.* 2 (2009) 175–188.
- [23] H. Ashassi-Sorkhabi, E. Asghari, Effect of hydrodynamic conditions on the inhibition performance of *L*-methionine as a “green” inhibitor, *Electrochim. Acta* 54 (2008) 162–167.
- [24] X. Jiang, Y.G. Zheng, W. Ke, Effect of flow velocity and entrained sand on inhibition performances of two inhibitors for CO₂ corrosion of N80 steel in 3% NaCl solution, *Corros. Sci.* 47 (2005) 2636–2658.
- [25] M. Boris, Y. Alla, A. Margarita, Effectiveness of corrosion inhibitors for the petroleum industry under various flow conditions, in: NACE international, Peoria, 2009.
- [26] N. 1D196, Laboratory test methods for evaluating oilfield corrosion inhibitors, in: Standard Practice, NACE international, Houston, 1996.
- [27] M. Bonis, M. Girgis, K. Goerz, R. MacDonald, Weight loss corrosion with H₂S: using past operations for designing future facilities, in: NACE International, Grand Rapids, 2006.
- [28] S. Smith, M. Joosten, Corrosion of carbon steel by H₂S in CO₂ containing environments, in: NACE international, Grand Rapids, 2006.
- [29] E. McCafferty, Validation of corrosion rates measured by the Tafel extrapolation method, *Corros. Sci.* 47 (2005) 3202–3215.
- [30] Q. Qu, L. Li, W. Bai, S. Jiang, Z. Ding, Sodium tungstate as a corrosion inhibitor of cold rolled steel in peracetic acid solution, *Corros. Sci.* 51 (2009) 2423–2428.
- [31] D.B. Kudryavtsev, A.R. Panteleeva, A.V. Yurina, S.S. Lukashenko, Y.P. Khodyrev, R.M. Galiakberov, D.N. Khaziakhmetov, L.A. Kudryavtseva, Polymeric inhibitors of hydrogen sulfide corrosion, *Petrol. Chem.* 49 (2009) 193–198.
- [32] H. Ma, X. Cheng, G. Li, S. Chen, Z. Quan, S. Zhao, L. Niu, The influence of hydrogen sulfide on corrosion of iron under different conditions, *Corros. Sci.* 42 (2000) 1669–1683.
- [33] J. Tang, Y. Shao, J. Guo, T. Zhang, G. Meng, F. Wang, The effect of H₂S concentration on the corrosion behavior of carbon steel at 90 °C, *Corros. Sci.* 52 (2010) 2050–2058.
- [34] R. Babić, M. Metikoš-Huković, Spectroelectrochemical studies of protective surface films against copper corrosion, *Thin Solid Films* 359 (2000) 88–94.
- [35] B.A. Boukamp, A nonlinear least squares fit procedure for analysis of admittance data of electrochemical systems, *Solid State Ionics* 20 (1986) 31–44.
- [36] H. Hamdy, Perchlorate and oxygen reduction during Zn corrosion in a neutral medium, *Electrochim. Acta* 51 (2006) 5966–5972.
- [37] B. Hirschorn, M.E. Orazem, B. Tribollet, V. Vivier, I. Frateur, M. Musiani, Determination of effective capacitance and film thickness from constant-phase-element parameters, *Electrochim. Acta* 55 (2010) 6218–6227.
- [38] A.K. Singh, M.A. Quraishi, Effect of Cefazolin on the corrosion of mild steel in HCl solution, *Corros. Sci.* 52 (2010) 152–160.
- [39] F. Bentiss, M. Traisnel, M. Lagrenée, The substituted 1,3,4-oxadiazoles: a new class of corrosion inhibitors of mild steel in acidic media, *Corros. Sci.* 42 (2000) 127–146.
- [40] E.A. Noor, Evaluation of inhibitive action of some quaternary *N*-heterocyclic compounds on the corrosion of Al–Cu alloy in hydrochloric acid, *Mater. Chem. Phys.* 114 (2009) 533–541.
- [41] E. McCafferty, Introduction to Corrosion Science, Springer Science, New York, 2010.
- [42] L. Cáceres, T. Vargas, L. Herrera, Determination of electrochemical parameters and corrosion rate for carbon steel in un-buffered sodium chloride solutions using a superposition model, *Corros. Sci.* 49 (2007) 3168–3184.
- [43] H. Amar, J. Benzakour, A. Derja, D. Villemin, B. Moreau, A corrosion inhibition study of iron by phosphonic acids in sodium chloride solution, *J. Electroanal. Chem.* 558 (2003) 131–139.
- [44] H. Ashassi-Sorkhabi, E. Asghari, Influence of flow on the corrosion inhibition of St52-3 type steel by potassium hydrogen-phosphate, *Corros. Sci.* 51 (2009) 1828–1835.
- [45] H.S. Klapper, D. Laverde, C. Vasquez, Evaluation of the corrosion of UNS G10200 steel in aerated brines under hydrodynamic conditions, *Corros. Sci.* 50 (2008) 2718–2723.
- [46] M. Saremi, C. Dehghanian, M. Mohammadi Sabet, The effect of molybdate concentration and hydrodynamic effect on mild steel corrosion inhibition in simulated cooling water, *Corros. Sci.* 30 (2006) 1404–1412.
- [47] B.R. Tian, Y.F. Cheng, Electrochemical corrosion behavior of X-65 steel in the simulated oil sand slurry. I: Effects of hydrodynamic condition, *Corros. Sci.* 50 (2008) 773–779.
- [48] G. Moretti, F. Guidi, Tryptophan as copper corrosion inhibitor in 0.5 M aerated sulfuric acid, *Corros. Sci.* 44 (2002) 1995–2011.

- [49] H. Ashassi-Sorkhabi, B. Shaabani, D. Seifzadeh, Effect of some pyrimidinic Schiff bases on the corrosion of mild steel in hydrochloric acid solution, *Electrochim. Acta* 50 (2005) 3446–3452.
- [50] L. Xianghong, M. Guannan, Tween-40 as corrosion inhibitor for cold rolled steel in sulphuric acid: weight loss study, electrochemical characterization, and AFM, *Appl. Surf. Sci.* 252 (2005) 1254–1265.